journal

J. Am. Ceram. Soc., 86 [8] 1370–78 (2003)

Abrasive Wear Behavior of Heat-Treated ABC-Silicon Carbide

Xiao Feng Zhang,*,† Gun Y. Lee,‡ Da Chen,¶,†† R. O. Ritchie,†,§ and Lutgard C. De Jonghe*,†,§

Materials Sciences Division, Lawrence Berkeley National Laboratory, University of California, Berkeley, California 94720

Department of Mechanical Engineering, University of California, Berkeley, California 94720

Department of Materials Science and Engineering, University of California, Berkeley, California 94720

Department of Materials Science and Engineering, Shanghai Jiao Tong University, Shanghai 200030, China

Hot-pressed silicon carbide, containing aluminum, boron, and carbon additives (ABC-SiC), was subjected to three-body and two-body wear testing using diamond abrasives over a range of sizes. In general, the wear resistance of ABC-SiC, with suitable heat treatment, was superior to that of commercial SiC. When the fine-scale (3 μm) diamond abrasives were used, it was found that thermal annealing at 1300°C increased the resistance to three-body wear by a factor of almost three, and two-body wear by a factor of almost two, compared with as-hot-pressed samples. Higher annealing temperatures, however, led to a decline in wear resistance from its highest value. Similar behavior was seen for 1300°C-annealed samples subjected to 15 μm diamond abrasive, although higher-temperature annealing at 1500°–1600°C enhanced the wear resistance again. When coarse abrasives (72 μm) were used, the wear resistance progressively increased with increased annealing temperature from ~1000° to 1600°C. Corresponding transmission and scanning electron microscopy studies indicated that, whereas transgranular, conchoidal cracking was dominant in the mild abrasive wear with fine-scale (3 μm) abrasives, intergranular cracking and subsequent grain pull-out was far more predominant in the more severe abrasive wear with coarse abrasives. Because the hardness and indentation toughness were barely altered during thermal treatment, the observed wear behavior was attributed mainly to the thermally induced microstructural changes, including the crystallization of glassy grain-boundary films, the possible strengthening of the boundaries due to the enhancement of the aluminum, and the formation of aluminum-rich, coherent nanoscale precipitates in the matrix grains above 1300°C.

I. Introduction

THE application of high-performance ceramics at elevated temperatures requires a high degree of chemical stability and excellent resistance to structural deformation, fracture, wear, and erosion. Enhanced strength, hardness, toughness, and creep resistance are of critical importance for components proposed for use in gas turbines, piston engines, heat exchangers, and aerospace applications. Exceptional hardness and wear resistance are also desired for ceramic materials used in brake linings, electrical contacts, and high-speed and high-precision cutting tools.

Among the various classes of high-temperature structural ceramics, hot-pressed, monolithic silicon carbide (SiC) may be one of the most attractive. Recent efforts have led to the successful *in situ* toughening of hot-pressed SiC containing aluminum, boron, and carbon (ABC-SiC), where large crack fracture toughness, K_{IC}, values as high as 9.1 MPa·m$^{1/2}$ have been achieved,[1–3] i.e., approaching that of self-reinforced Si_3N_4.[4] This is to be compared with commercial SiC ceramics, where K_{IC} values are characteristically <5 MPa·m$^{1/2}$. This remarkable increase in toughness has been attributed to resistance-curve (*R*-curve) behavior from grain bridging in the crack wake induced by the structural evolution of the grain-boundary films. Whereas grain boundaries in polycrystalline ceramics often contain a thin layer of amorphous material,[5–9] extensive transmission electron microscopy (TEM) characterization has revealed that the grain-boundary films in the hot-pressed ABC-SiC can be crystallized during heat treatment.[9] High-resolution TEM also has detected the presence of aluminum-rich nanoscale precipitates formed above ~1300°C during post-annealing heat treatments.[10,11] These changes in microstructure can be expected to affect the wear resistance of ABC-SiC.

The object of this article is to study the effect of post-hot-pressing heat treatments on the abrasive wear behavior of hot-pressed monolithic ABC-SiC. It has been found that the wear resistance of ABC-SiC is quite sensitive to annealing treatments above 1000°C and can be almost tripled by annealing at 1300°C to exceed that of a commercial SiC (Hexoloy SA, Saint-Gobain Advanced Ceramics Corp., Niagara Falls, NY).

II. Experimental Procedures

(1) Materials Preparation

Dense SiC was prepared by hot-pressing submicrometer β-SiC powders (H. C. Starck, Goslar, Germany) mixed with 3 wt% aluminum (metal) (~5 μm diameter powder, H-3 and H-10, Valimet, Stockton, CA), 0.6 wt% boron (Callery Chemical Co., Callery, PA), and 2 wt% carbon. Carbon was introduced as Apiezon wax (AVO Biddle Instruments, Blue Bell, PA) dissolved in toluene. The other powders were then added to the suspension, which was subsequently agitated using an ultrasonic probe for 10 min to minimize agglomerate formation. The resulting slurry was stir dried, and the material was ground in a mortar and pestle before sieving through a 200 mesh screen.

The green samples were precompacted using a 35 MPa die pressure. For hot pressing, three samples were inserted into a graphite die lined with graphite foil. Graphite spacers were placed between each of the three samples. The hot-press furnace was heated *in vacuo* to ~400°C overnight, and then brought to the hot-pressing temperature of 1900°C at a rate of 10°C/min. A load of 50 MPa, a hot-pressing time of 1 h, and flowing argon gas were

D. B. Marshall—contributing editor

Manuscript No. 186892. Received June 19, 2002; approved March 31, 2003.

Supported by the Director, Office of Science, Office of Basic Energy Sciences, Division of Materials Sciences and Engineering of the U.S. Department of Energy under Contract No. DE-AC03–76SF0098.

*Member, American Ceramic Society.

†Materials Sciences Division, Lawrence Berkeley National Laboratory.

‡Department of Mechanical Engineering, University of California.

§Department of Materials Science and Engineering, University of California.

¶Department of Materials Science and Engineering, Shanghai Jiao Tong University.

††Deceased.

used. After the samples were hot-pressed, the furnace was naturally cooled down to room temperature. The hot-pressed products consisted of 4 mm thick, 38 mm diameter disks, with a density of 3.18 g/mm^3. One surface of the disks was polished to a 1 μm finish before the samples were sectioned for mechanical testing and characterization using scanning (SEM) and transmission electron microscopies.

Individual samples were postannealed for 72 h in argon at a series of temperatures, in 100°C intervals, between 1000° and 1600°C. All postannealing treatments, wear tests, and structural characterizations were performed on separate beams sectioned from the same as-hot-pressed disk.

(2) Abrasive Wear Testing

Two different configurations (tribosystems) were used for the three-body and the two-body abrasive wear testing. The first of these involved three-body, wheel-on-disk abrasive wear, as shown schematically in Fig. 1(a). Specifically, a 3 mm wide, 15 mm diameter stainless-steel wheel was run at a constant rotational speed and contacted onto immobile 4 mm × 3 mm× 3 mm SiC plate-shaped samples, immersed in a slurry of 3–15 μm diameter diamond particles suspended in water. The second wear setup allowed for two-body, pin-on-wheel abrasive wear testing, in which a cross-sectional surface of a 15 mm × 3 mm × 3 mm SiC beam was brought into contact with the surface of a diamond abrasive wheel without lubrication (Fig. 1(b)). The wheel, 150 mm in diameter, was dressed with diamond coatings containing either 3, 15, or 72 μm diameter diamond particles (dressing sticks: NDL stick + MDS 38, National Diamond Laboratory, Los Angeles, CA). All wear experiments were performed in air, at ambient temperature.

Wear was characterized by the specific wear rate, K_w, defined in units of mm^3/(N·m) as the volume of material removed per unit sliding distance per unit load:

$$K_w = \frac{V_w}{PS} \tag{1}$$

where V_w is the worn volume of the sample, P the applied normal load, and S the sliding distance. Based on this relationship, the wear resistance is defined as $1/K_w$.

For the three-body wear experiments (Fig. 1(a)), the contact load P was 1 N, over a distance S of 11 000 m at a sliding speed of 1 m/s. For the two-body wear experiments (Fig. 1(b)), the contact load was $P = 2$ N, over a distance of $S = 1005$ m at a sliding speed of 0.15 m/s.

The temperature increase on the contact surface was negligible because of the relatively low sliding speeds and high thermal conductivity of the SiC (e.g., 126 W/(m·K) for commercial SiC (Hexoloy SA)). The value of the wearing volume, V_w, was computed from the SiC density and the weight loss; the latter was measured using a microbalance to a precision of 0.001 g. The wear rate of identical samples can vary considerably when tribosystems and conditions are different.[12] Accordingly, although relative trends can be compared, any quantitative comparison of the relative wear rates for these two types of wear-testing configurations is not very meaningful; for quantitative comparison, identical facilities and conditions must be used.

Equation (1) is fully applicable to the pin-on-wheel wear test (Fig. 1(b)), in which both of the contacted surfaces can be regarded as locally flat. In the wheel-on-disk wear test (Fig. 1(a)), the wear surface is concave, resulting in a nonuniform wear rate, such that the normal surface stress is distributed to maintain conformity with the wheel. In this case, a more appropriate definition for the specific wear rate is to use the wear depth, δ_w, per unit sliding distance per unit normal stress, such that the wear rate, $K'_w(\sigma)$, is given by

$$K'_w = \frac{\delta_w}{\sigma S} = \frac{\dot{\delta}_w}{\sigma v_w} \tag{2}$$

where $\dot{\delta}_w$ is the depth of the wear per unit time, σ the contact stress (normal load per unit area), and v_w the sliding velocity. However, such subtleties are not explicitly addressed in this work.

(3) Mechanical Properties

The room-temperature hardness, (indentation) fracture toughness, and modulus of rupture were obtained for all samples. A microhardness tester (Micromet, Bedford, MA) was used for hardness measurements. A low indentation load of 4.9 N (500 g) and an indenter dwell time of 15 s were applied to the 1 μm polished surfaces to control the indent-to-grain size ratio; a typical diagonal across the indents was ~19 μm, i.e., spanning several grains. A standard Vickers indentation with a load of 78.4 N (8 kg) was used for the indentation toughness measurements, again on the polished surfaces. Typical indent diagonals in this case were 70–80 μm, with ~100 μm of crack extension from the indent corners. Mean toughness values and their standard deviations were determined from 30 to 40 indents.

The room-temperature moduli of rupture were determined using unnotched, 40 mm × 3 mm × 3 mm beams, loading in four-point bending using a high-density graphite bending rig. The outer and inner loading spans were, respectively, 25.4 and 9.5 mm, and the test was conducted at a crosshead speed of 0.05 mm/min. Modulus of rupture values were obtained for the as-hot-pressed and thermally annealed samples.

(4) Electron Microscopy Characterization

To examine the microstructures using TEM, 3 mm diameter disks were cut from the SiC samples, ground, dimpled, and

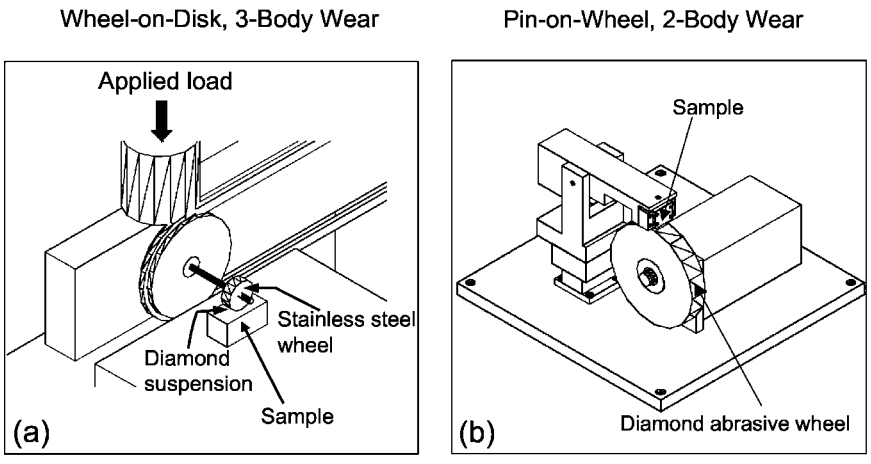

Fig. 1. Schematic illustrations of the tribological setups for the (a) wheel-on-disk three-body and (b) pin-on-wheel two-body wear tests.

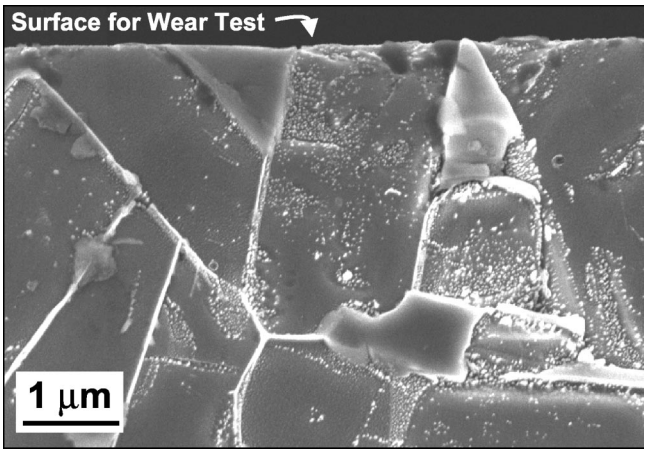

Fig. 2. Cross-sectional SEM micrograph showing the original SiC surface before wear, indicating that the sectioning and polishing do not introduce significant near-surface damage.

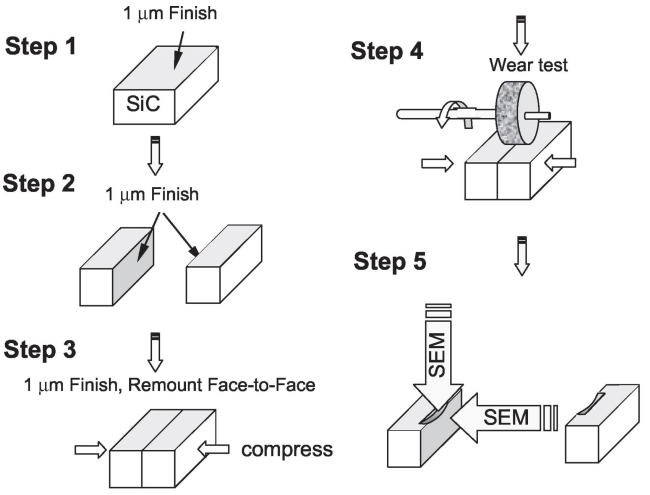

Fig. 3. Schematic illustration of the procedure used in preparation of cross-sectional SEM samples to study subsurface wear damage. An as-processed (prior-to-wear) sample was cut and then recombined, as shown in steps 2 and 3. Wear testing was performed (step 4), followed by cross-sectional and plane-view examinations of the worn surface using SEM (step 5).

polished, before being ion milled in an argon-ion beam to achieve electron transparency. TEM characterization was performed at the National Center for Electron Microscopy at the Lawrence Berkeley National Laboratory, using a transmission electron microscope (Model CM200, Philips, Eindhoven, The Netherlands) operating at 200 kV.

The topography and structure of the worn surfaces were imaged using SEM (Model JSM-6340F, JEOL, Tokyo, Japan) working at 5 kV. For the preparation of cross-sectional samples for SEM studies, as-processed (prior-to-wear) samples were cut along a plane perpendicular to the surfaces to be used for the wear test. The effect of possible cutting damage was minimized by removing a few micrometers from the cut surfaces by polishing. Figure 2 shows a SEM micrograph of a cross section before wear, in which the surface that has been polished for subsequent wear testing is marked by the arrow. The sectioning and polishing did not introduce significant near-surface damage. The two pieces were then recombined by a mechanical pushing force, as schematically illustrated in Fig. 3. This method is similar to that reported by Lawn *et al.*,[13] who used a thin layer of adhesive to bond the two pieces together. The surfaces were then subjected to three-body wear testing under the same conditions as described above, but for a sliding distance of 60 m with the direction of wear aligned along the joining line, which was centered in the middle of the wear track (Fig. 3). The worn surface was then cleaned in acetone and ethanol, and baked at 150°C for 10 min, before plasma etching for SEM observation.

III. Results

(1) Mechanical Properties and Wear Resistance

Vickers indentation hardness, indentation fracture toughness, and flexural strength values for the SiC samples before and after thermal annealing between 800° and 1600°C are plotted in Fig. 4. It is apparent that, whereas the hardness and indentation toughness are essentially unchanged by the annealing heat treatment, a marked increase is seen in flexural strength above ~1200°C.

The wear resistance ($1/K_w$) has been similarly determined for as-hot-pressed and thermally annealed SiC samples; results from three-body and two-body wear tests using a 3 μm diamond abrasive are plotted in Fig. 5. For comparison, wear data are also shown for as-received, commercial SiC (Hexoloy SA), which has been tested under identical conditions.

It is evident from Fig. 5 that the wear resistance of ABC-SiC is affected by thermal annealing. For 3 μm diamond abrasive, three-body and two-body wear tests show a continuously improving wear resistance when annealed between 1200° and 1300°C. After annealing at 1300°C, the three-body wear resistance is almost three times, and two-body wear resistance almost two times, the value for the unannealed material. However, on annealing at temperatures >1300°C, the wear resistance appears to decline. For comparison, similar wear tests also have been performed on the commercial SiC (Hexoloy SA). This material contains ~5 μm diameter equiaxed grains with no intergranular films. The fracture strength and toughness are measured to be 400 MPa and 2.8 MPa·$m^{1/2}$, respectively.[1] The plots in Fig. 5 show that the optimized wear resistance in ABC-SiC is superior to that of the as-received, commercial SiC material.

These trends, however, vary with the size of the diamond abrasive. Similar local maximums in the wear resistance values following annealing at 1300°C are also evident with the 15 μm diamond abrasive, although the peaks are not as pronounced as with the 3 μm abrasive. Moreover, the wear resistance starts to increase again on annealing above 1400°C. For the coarsest, i.e., 72 μm abrasive (Fig. 6), where only two-body wear has been characterized, the wear resistance starts to increase after annealing above 1000°C and increases progressively with increasing annealing temperature up to 1600°C, the maximum annealing temperature studied.

(2) Microstructure Characterization

The as-hot-pressed ABC-SiC is composed of elongated and equiaxed SiC grains, with 0.8–3 nm thick films of glassy phases at the

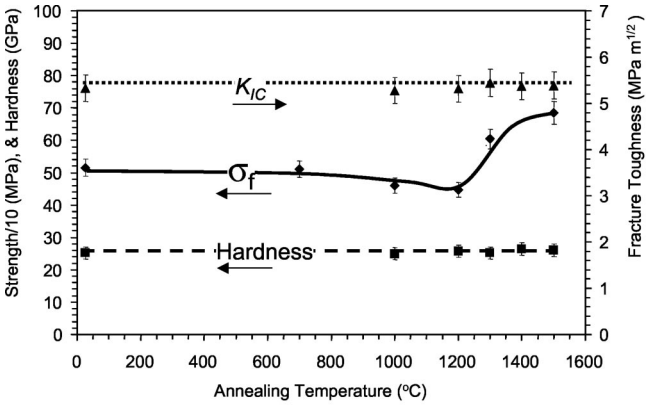

Fig. 4. Experimentally measured variation in indentation hardness, indentation toughness, K_{IC}, and flexural strength, σ_f, of ABC-SiC samples as a function of the annealing temperature between 800° and 1600°C.

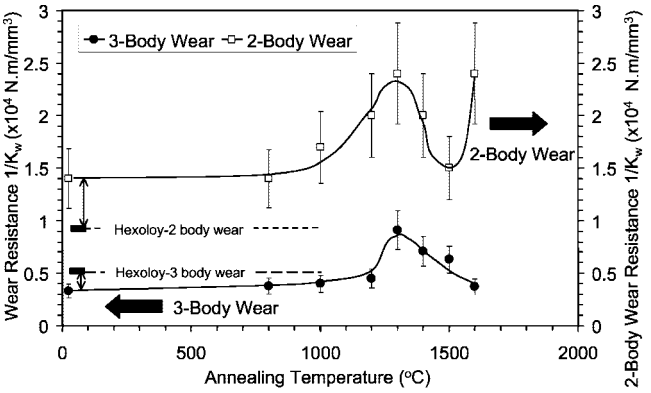

Fig. 5. Experimentally measured variation in three- and two-body wear resistance ($1/K_w$) as a function of the annealing temperature, using a 3 μm diamond abrasive.

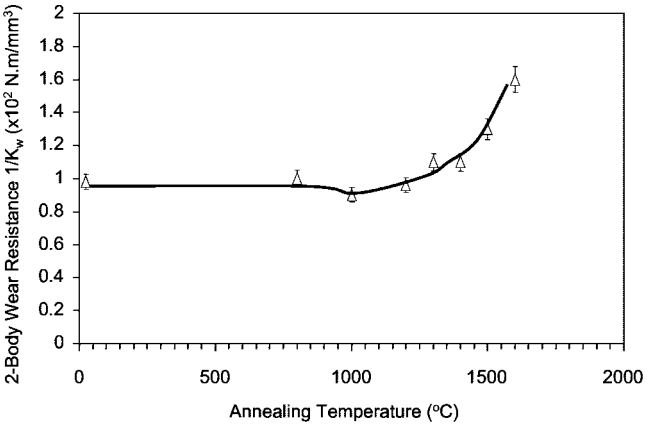

Fig. 6. Experimentally measured variation in two-body wear resistance ($1/K_w$) as a function of the annealing temperature, using a 72 μm diamond abrasive.

grain boundaries. The typical size for the equiaxed grains is <1 μm, whereas the length and width for anisotropic grains ranges, respectively, from 3 to 11 μm and 1 to 3 μm, with an aspect ratio for 90% of the elongated SiC grains between 2 and 5 (Fig. 2). X-ray and electron diffraction previously have identified the α-4*H* and α-6*H* hexagonal SiC phases as the dominant polytypes, and various aluminum-rich secondary phases exist in all samples studied.[9,14] After the samples were annealed at elevated temperatures, no noticeable changes in grain size and morphology were observed, as expected from the microstructure achieved in the as-processed samples.

As noted earlier, the thermal annealing treatment is found to result in several important microstructural changes. Crystallization of the grain-boundary films occurs after ~1 h at temperatures >1000°C. Figure 7(a) shows a typical amorphous intergranular film formed in as-hot-pressed ABC-SiC. Systematic TEM analyses indicate that the intergranular films are composed of Al-Si-O-C.[9] However, on annealing at ≥1000°C, the amorphous intergranular films were observed to crystallize (Fig. 7(b)). High-resolution electron microscopy and chemical microanalysis of the crystallized intergranular films identified one of the crystalline structures within the films as consistent with a 2*H*-wurtzite structure with an aluminosilicate composition, i.e., a solid solution between Al_2OC and SiC.[9] In addition, the precipitation of nanoscale aluminum-containing phases was found to occur within SiC grains, quite rapidly, above ~1300°C (Fig. 8); their size, shape, spacing, and volume fraction are listed in Table I. The precipitates are coherent and typically plate shaped. No such nanoprecipitates are observed in samples annealed at ≤1200°C. For a 72 h thermal anneal at 1300°C, approximately one-half to one-third of the aluminum dissolved in the SiC lattice was found to have precipitated out; indeed, isochronal annealing at ≥1400°C, for >72 h, led to the complete precipitation of almost all the dissolved aluminum. At the same time, aluminum was observed to accumulate in the grain boundaries, with the consequent formation of a precipitate-denuded zone of low aluminum concentration adjacent to the boundaries. Chemical analysis detected a 50–100 at.% increase in aluminum content in the grain-boundary films after annealing at and above 1300°C. The width of this denuded zone was found to increase with temperature. Concurrently, the aluminum-containing precipitates in the matrix coarsened at constant overall grain-bulk composition, as shown in Fig. 8 and in Table I. A detailed TEM study of such nanoprecipitation is given in Refs. 10 and 11.

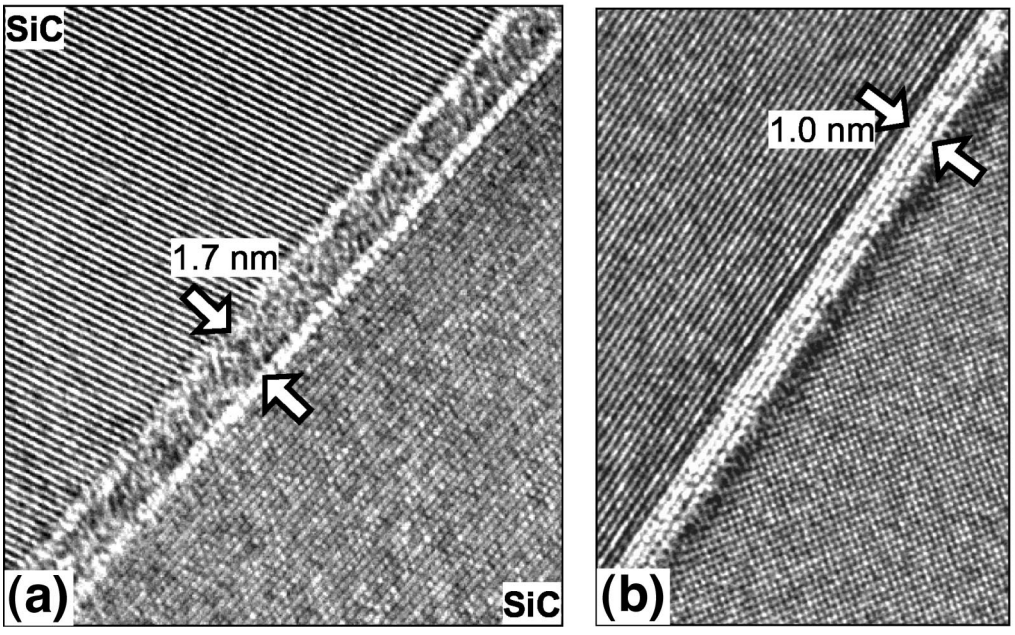

Fig. 7. TEM micrographs showing the transformation of the amorphous grain-boundary film (a) to a crystallized film (b) after thermal annealing at 1000°C for 5 h. Grain boundaries shown in (a) and (b) are not the same boundary.

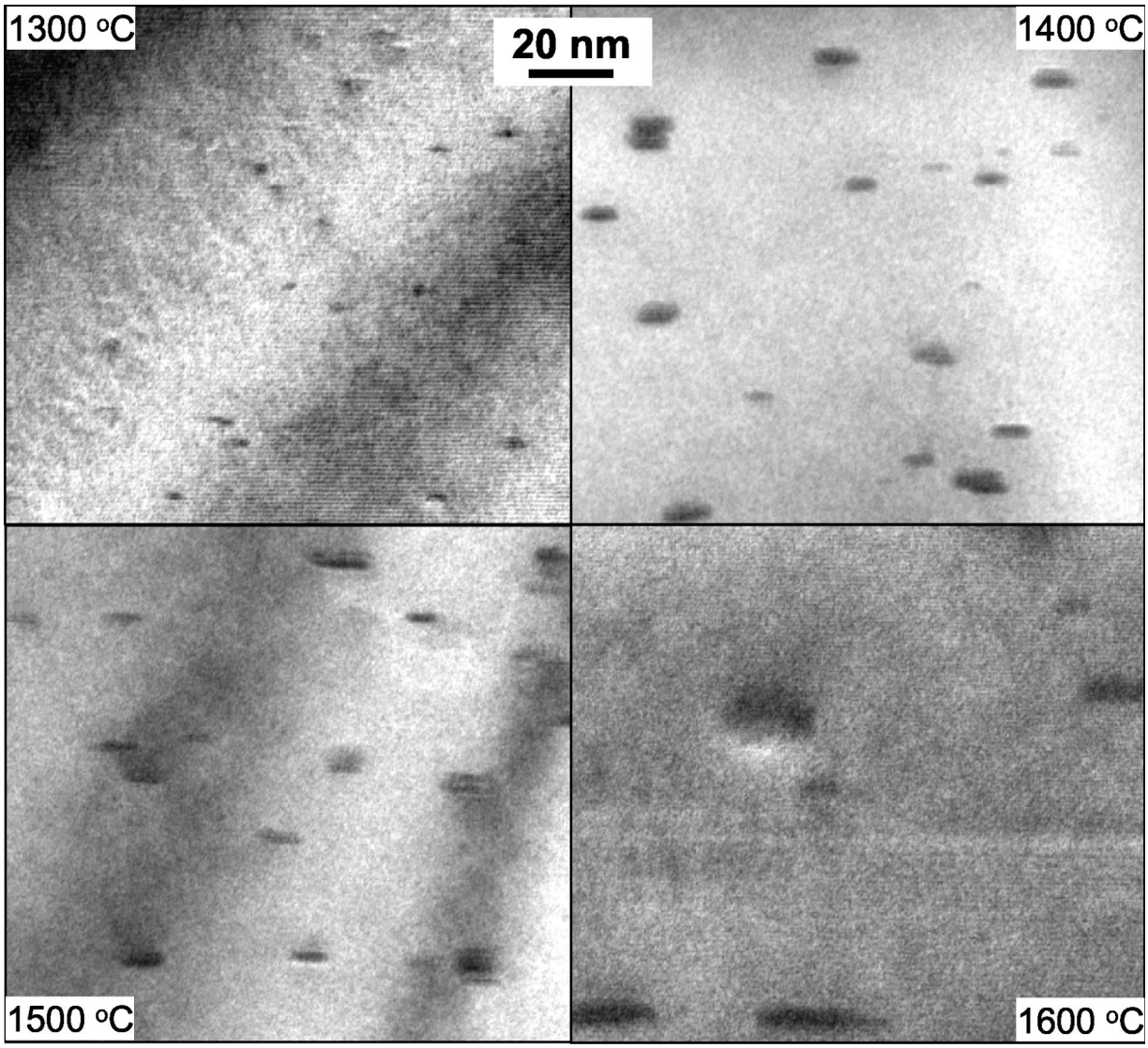

Fig. 8. TEM micrographs showing in-grain nanoprecipitates in ABC-SiC annealed at 1300°, 1400°, 1500°, and 1600°C. Note the coarsening in size accompanied by number decrease of the precipitates with increasing annealing temperature.

Table I summarizes the statistical values for the precipitates formed at various annealing temperatures. The typical length and thickness for the precipitates produced in the 1300°C-annealed samples are between 3 and 5 nm, and ~1 nm, respectively. The minimum separation is ~2 nm. The average volume of the individual precipitates is ~16 nm^3, and a number density of ~5×10^{22} $/m^3$ has been determined. It is apparent that isochronal annealing between 1400° and 1600°C coarsened the precipitates significantly.

(3) Characterization of the Worn Surfaces

Considering first the fine-scale abrasives, high-magnification, plane-view SEM images, obtained from the as-hot-pressed ABC-SiC, are shown in Fig. 9. The SiC surface after two-body wear with 3 μm diamond abrasive can be seen. Several features can be discerned, most prominently the occurrence of polishing wear and the presence of pits resulting from the break out of individual or groups of grains (Fig. 9(a)). Close-ups of the light-contrast features associated with many of the pits are shown in Figs. 9(b) and (c)

Table I. Experimentally Measured Data for the Platelike Nanoscale Precipitates Formed within SiC Grains in the Annealed ABC-SiC†

Nanoprecipitate property	Annealing temperature (ABC-SiC) (°C)			
	1300	1400	1500	1600
Length (nm)	4.6 ± 0.9	9.8 ± 0.3	11.8 ± 2.4	21.1 ± 7.6
Thickness (nm)	1.2 ± 0.1	3.9 ± 1.3	4.0 ± 1.2	5.5 ± 1.4
Aspect ratio	3.8 ± 1.2	2.7 ± 1.0	3.1 ± 1.0	4.0 ± 1.6
Separation (nm)	6.4 ± 3.6	17.9 ± 5.6	19.8 ± 7.9	38.6 ± 16.4
Volume (nm^3)	16	300	428	2200
Number density ($1/m^3$)	5×10^{22}	1×10^{22}	7×10^{21}	2×10^{21}
Volume fraction‡	0.8×10^{-3}	3.0×10^{-3}	3.0×10^{-3}	4.4×10^{-3}

†Statistical mean values and standard deviations are listed. ‡Volume fraction = mean volume × number density.

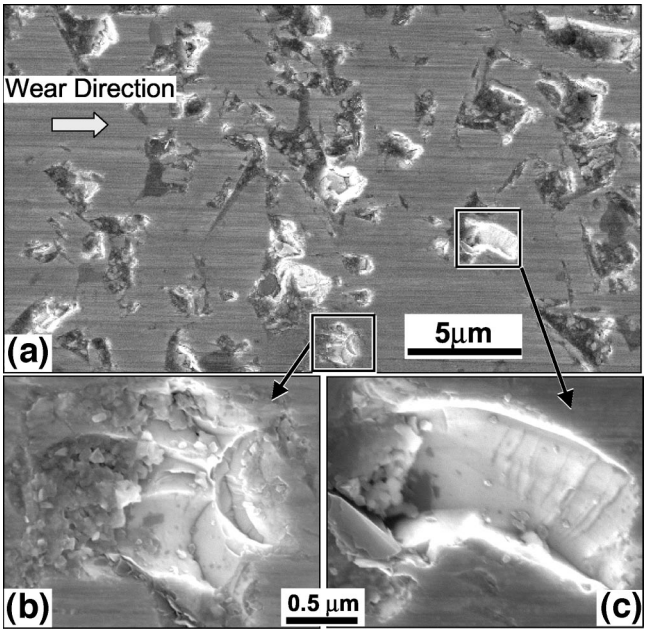

Fig. 9. Plane-view SEM images of the morphologies of the worn surfaces after two-body abrasive wear with 3 μm diamond abrasives, showing (a) an overall image and (b) and (c) high-magnification details of the light-contrast pits, which demonstrate transgranular, conchoidal fracture. Images were obtained from an as-hot-pressed sample.

and can be seen to consist of transgranular, conchoidal fracture surfaces. Similar features have been found in wear and contact fatigue studies of glasses[15] and other ceramics.[16]

The SEM micrographs in Figs. 10(a) and (b) compare plane-view images of the worn surfaces after the two-body, 3 μm diamond abrasive wear tests for as-hot-pressed and 1300°C-annealed samples. Polishing features are again common on the worn surfaces, together with dark-contrast pits due to grain break out. One striking difference between the samples is that the grain break out and the conchoidal fractures (light-contrast pits) are significantly decreased following thermal annealing. At a minimum, the decrease in grain break out lowers the normal stress for the remaining, load-bearing surface. The wear surface of the annealed sample in Fig. 10(b) shows that the light-contrast conchoidal fracture features in this sample are localized in a 15–20 μm wide band in the wear direction, suggesting that these features are associated with wear damage that is caused by debris released by the sample.

Corresponding worn surfaces due to coarse-scale abrasive are shown in Figs. 11(a) and (b) in the form of SEM plane-view images after two-body wear tests with 72 μm diamond abrasive. Unlike behavior with fine-scale abrasive (Fig. 10), the worn surfaces for the as-hot-pressed and 1300°C-annealed SiC samples are quite similar. Polishing-type features are no longer present, and the surface features indicate a combination of intergranular (some are marked by arrows) and transgranular fractures.

Thus, whereas wear with fine-scale abrasive appears to involve predominately local trangranular fracture processes, coarse abrasive appears to involve intergranular and transgranular processes. However, cross-sectional SEM observations indicate that all worn samples show some degree of near-surface fractures, and intergranular cracking also can be seen with three-body wear with 3 μm abrasives (Fig. 12). Moreover, the incidence of such near-surface intergranular cracking increases with increasing abrasive size. For example, Fig. 13 shows the corresponding near-surface damage and fractures after three-body wear with 15 μm abrasives. The black arrows in three images at the top indicate the fracture paths initially involve intergranular failure before proceeding transgranularly.

IV. Discussion

The major characteristic of the three- and two-body abrasive wear properties of ABC-SiC studied in this work is the significant improvement in wear resistance that can be achieved by thermal annealing at and above 1300°C. This increase in the wear resistance is such that, when optimized, ABC-SiC can have superior wear properties to commercial SiC (Hexoloy SA); indeed, ABC-SiC after suitable annealing displays a wear resistance that has a factor of two or more higher than (as-received) commercial SiC (Hexoloy SA) under identical testing conditions. However, the precise wear behavior of ABC-SiC depends critically on the scale of the abrasive, specifically in relation to the characteristic size-scales of the microstructural changes involved. For the thermally annealed samples, depending on the temperature of the isochronal anneals, the wear resistance increases most significantly for the case of mild abrasive wear with smaller particle abrasives (less than ~20 μm), although there are certain annealing temperature regimes where the change of the wear resistance is not significant.

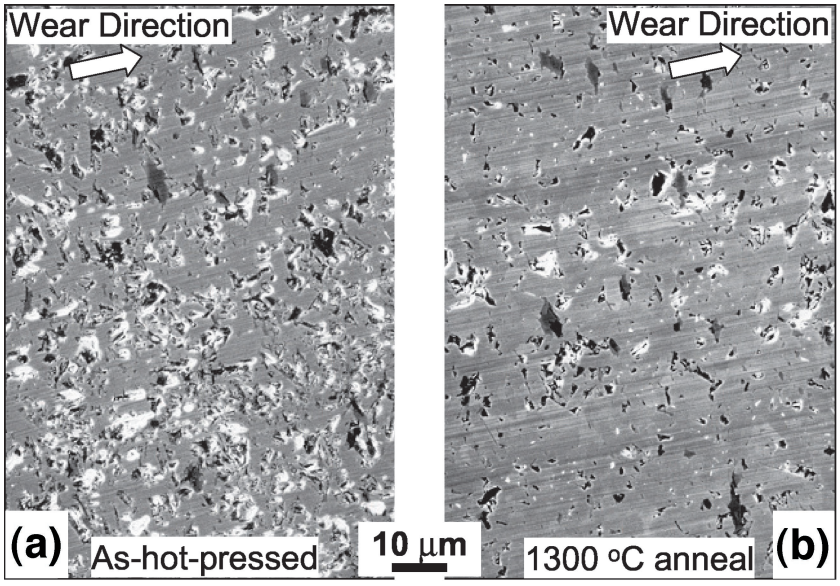

Fig. 10. Plane-view SEM images showing the morphologies of the worn surfaces after two-body abrasive wear with 3 μm diamond abrasives, showing (a) as-hot-pressed and (b) 1300°C-annealed ABC-SiC, showing decrease in pitting due to the annealing.

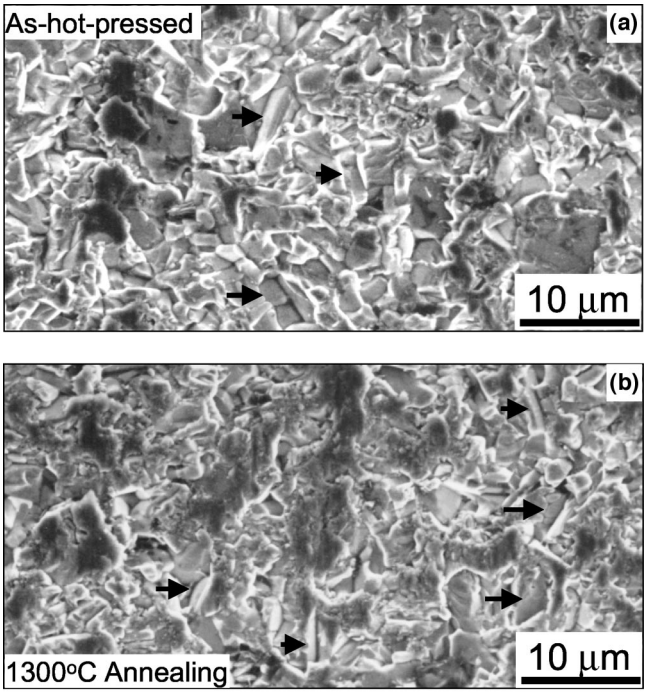

Fig. 11. Plane-view SEM images showing the morphologies of the worn surfaces after two-body abrasive wear with 72 μm diamond abrasives. Image in (a) was obtained from the as-hot-pressed ABC-SiC and that in (b) was from the sample after 1300°C annealing.

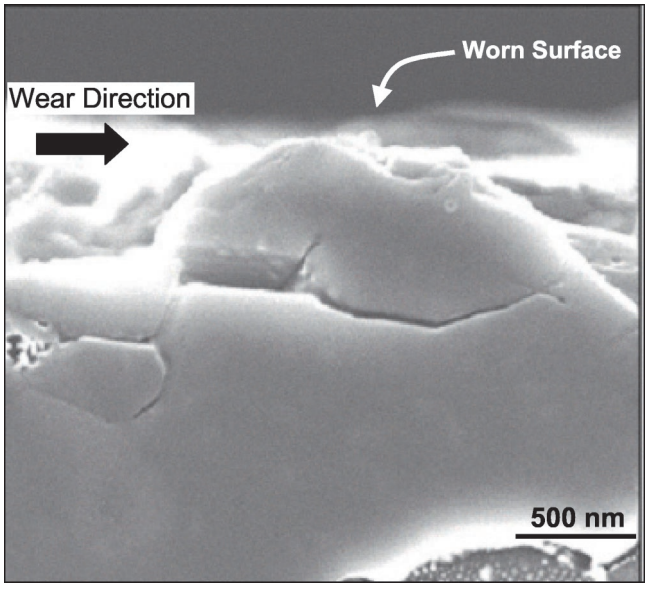

Fig. 12. Cross-sectional SEM micrograph of the near-surface structure of the worn surface after three-body wear with 3 μm diamond abrasives, showing the presence of an intergranular crack. Sample was annealed at 1300°C before the wear test.

Remarkably, this variation in wear behavior does not correlate with changes in indentation fracture toughness or hardness; indeed, both the latter properties are essentially insensitive to the thermal annealing treatments. This at first sight may seem unusual, because main materials properties that determine wear behavior are usually taken to be the hardness and (more prominently in brittle materials) the fracture toughness. However, one factor here is that the fracture toughness of ABC-SiC is largely controlled by crack-tip shielding, in the form of interlocking grain bridging, in the crack wake, which introduces *R*-curve behavior. This is a large-crack material property that requires a crack wake of many grains to develop the full effect of the extrinsic toughening.[2] The large-crack material property is expected to have little relevance to the "small-crack" cracking behavior associated with the observed wear mechanism, where, conversely, the cracking of the matrix and the boundaries takes place over dimensions comparable with a single-grain, or even subgrain, size scales.

Another striking feature of the wear behavior in ABC-SiC is the appearance of a local maximum in wear resistance after 1300°C annealing for small-particle abrasion, in particular that shown by the 3 μm wear data for three- and two-body wear. This local maximum is much decreased in prominence at larger abrasive particle sizes, i.e., for ≥15 μm abrasive. Because these effects are not associated with variations in indentation fracture toughness or hardness, the origin of these local variations in wear behavior therefore must be associated with the microstructural evolution of ABC-SiC during annealing, including a decrease in the residual stress resulting from thermal expansion anisotropy during cooling from the processing temperature,[17] crystallization of the boundary films, possible changes in the grain-boundary strength, healing of flaw damage, and the formation and coarsening of the nanoprecipitates in SiC grains.

(1) Mild Wear (Fine Abrasives)

For the case of the mild abrasive wear with the fine-scale (3 μm) abrasives, the wearing surface topology that develops shows microplowing, limited grain removal, and associated fractures, with the actual load-bearing surface remaining relatively smooth and exhibiting microplastic wear (Figs. 9 and 10); similar observations of such mechanisms have been reported in Refs. 18 and 19. There is far less evidence of intergranular cracking here, and transgranular, conchoidal cracking damage is the most common mechanism that can be seen on the worn surfaces, as shown schematically in Fig. 14(a). Microplowing and transgranular near-surface crack formation appear to be the predominant sources of the wear debris. Because the affected volumes in microplowing wear of SiC are quite small, it can be expected that this type of wear is affected by the matrix (rather than the boundary) properties and the presence of the nanoprecipitates, with a behavior somewhat similar to precipitation hardening in metals and alloys. The expectation is confirmed by the fact that a good correlation exists between the formation of well-dispersed, very fine precipitates and the appearance of the local wear-resistance maximum after annealing at 1300°C. However, just as the dispersion-hardening effect is weakened by coarsened precipitates in metals and alloys, the overaging of the precipitates in ABC-SiC at annealing temperatures >1300°C coarsens the nanoprecipitates (Fig. 8), resulting in decline of the wear resistance from the local maximum. Our experimental data suggest that the beneficial effect of the thermal annealing in promoting wear resistance can be attributed to reinforcement of the SiC grains through the formation of nanoscale precipitates with a suitable size and number density, although their coarsening may lead to a local decrease in wear resistance.

(2) Severe Wear (Coarse Abrasives)

For the severe abrasive wear associated with the coarse (72 μm) abrasive, where the dimensions of the abrasive are far in excess of microstructural size-scales, the wear surfaces appear quite different and show evidence of severe and deep damage. Here, grain pullout and intergranular cracking predominate, with an incidence rate that decreases with increasing annealing temperature. Grain-boundary-initiated fractures and subsequent grain break out through conchoidal cracking (Fig. 14(b)), with a smaller degree of transgranular fracture and grain shattering, are the main near-surface damage mechanisms (Fig. 11). Grain-fragment break out is a result of continued distress from the incompatibility of intergranular cracks at triple junctions under intensive sliding by the abrasive medium. The degree of such distress is enhanced at larger abrasive size, as shown by the cross-sectional SEM images in Fig.

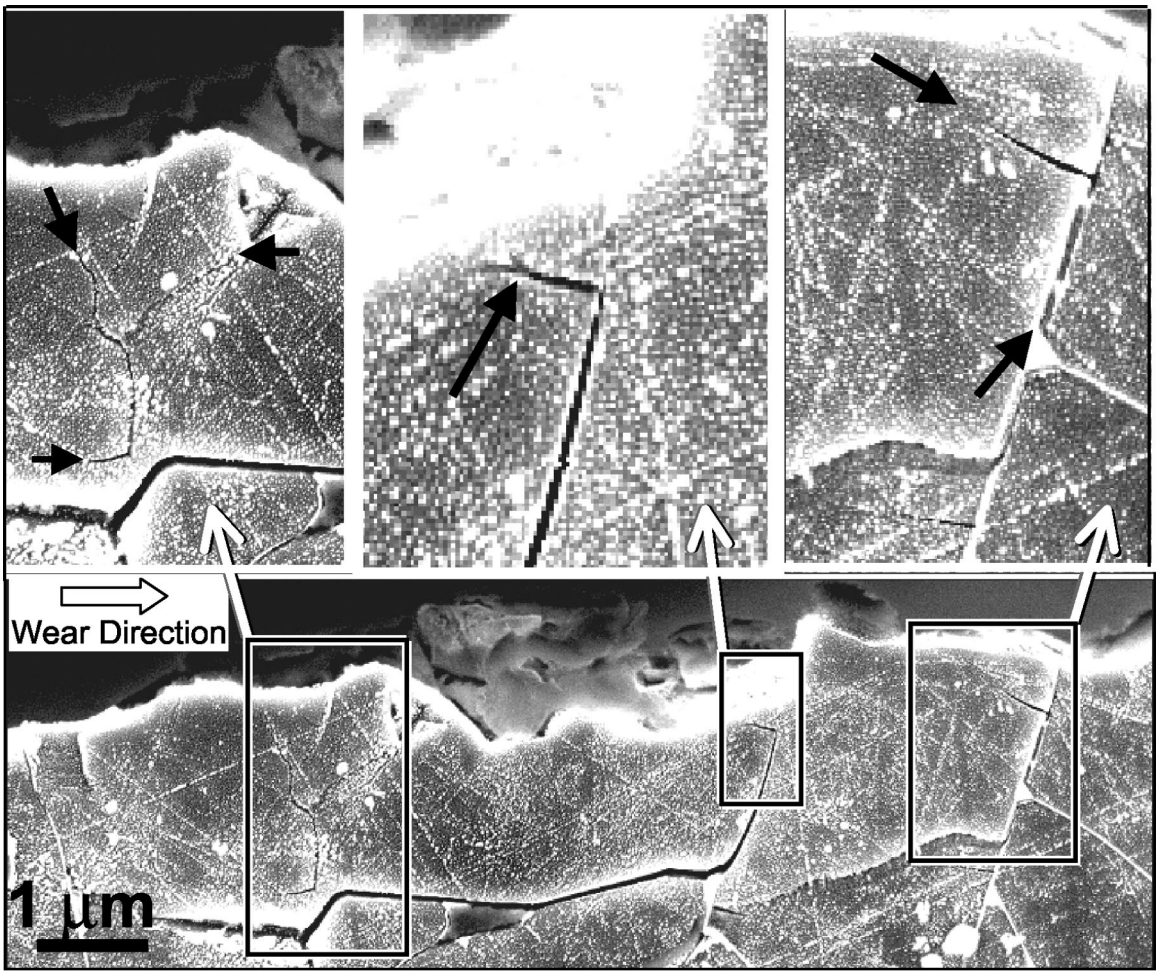

Fig. 13. Cross-sectional SEM micrographs of the near-surface structure of the worn surface after three-body wear with 15 μm diamond abrasives. Arrows in three images at the top indicate that the near-surface fracture path initially involves intergranular failure before proceeding transgranularly. Sample was annealed at 1300°C before the wear test.

15 for three-body wear of a 800°C-annealed sample with 15 μm abrasive. The enhanced damage with the coarser abrasive can cause near-surface grain segments to be completely shattered, to a depth of ~5 μm below the surface.

Such grain break-out processes are not expected to be affected by the matrix-coherent precipitates that are orders of magnitude smaller than the fracture features. Thus, in contrast to the wear mechanism in the fine-particle abrasive wear regime, the removal of material in the coarse-particle abrasive wear regime is thought to be determined more by the grain-boundary properties, and possibly by the residual stress decrease and flaw healing. The measured increase in the modulus of rupture on annealing (Fig. 4) is perhaps an indication of the decrease in residual stresses and of possible flaw healing, although the relative increase in the modulus of rupture is significantly less than the relative increase in the wear resistance. It is therefore postulated that the increase in wear resistance is associated with the strengthening of the grain boundaries, which clearly tends to inhibit intergranular fracture. Although no conclusive evidence for such strengthening has been achieved, either experimentally or theoretically, in SiC, as described above in Section III(2), we have detected a dramatic increase (50–100 at.%) in aluminum content in the grain-boundary films after high-temperature annealing, and this effect is known to lead to grain-boundary strengthening in comparable ceramics, such as in Si_3N_4.[20] Although the grain-boundary strengthening tends to inhibit the intergranular fracture, it may at the same time enhance the potency of the grain bridging in the wake of the crack. This competition between the two effects causes no appreciable change in indentation toughness.

V. Conclusions

Based on an experimental study of the role of postprocessing heat treatment on the three- and two-body abrasive wears of an *in*

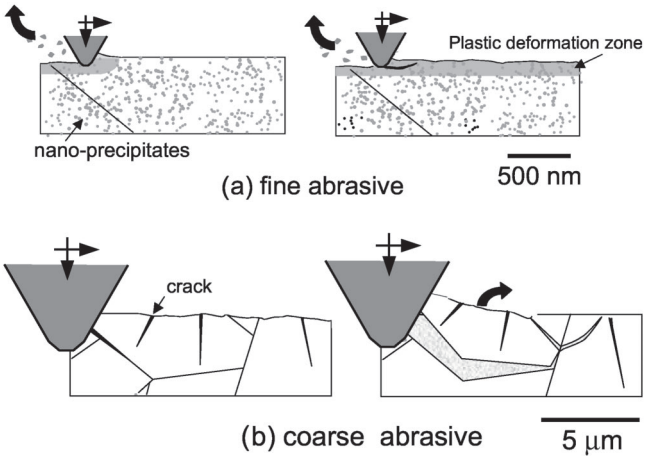

Fig. 14. Schematic illustration of the sequences of events in the formation of wear debris for (a) mild wear with fine abrasives and (b) severe wear with coarse abrasives. Note that, whereas the mechanism of wear with fine abrasives involves microplowing and near-surface cracking, with coarse abrasives, intergranular cracking and grain pullout, e.g., represented by the break-out of the grain fragment in (b), are the more dominant mechanisms.

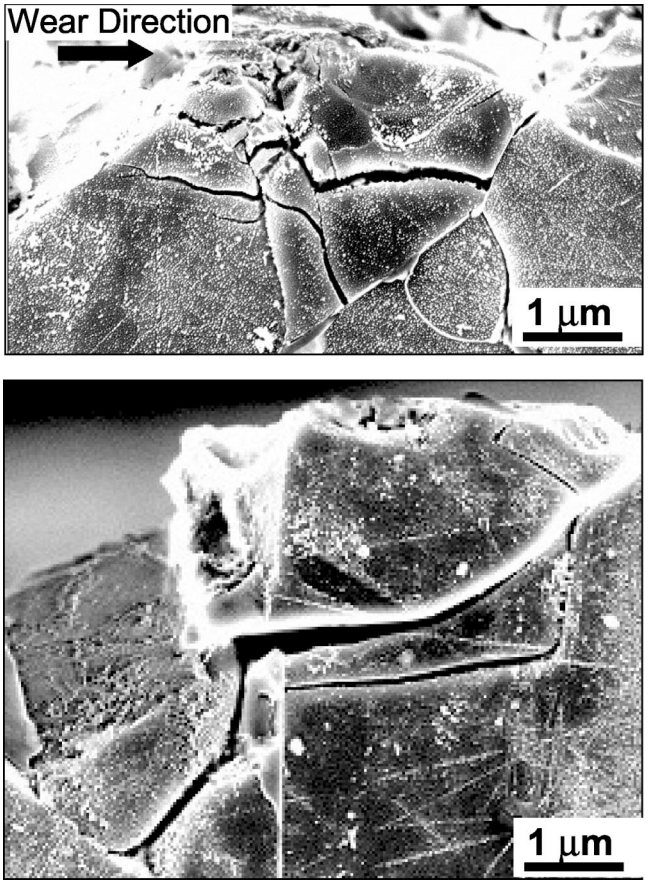

Fig. 15. Cross-sectional SEM micrographs of the near-surface structure of the worn surface after three-body wear with 15 μm diamond abrasives, showing near-surface damage, in the form of grain segments, to be completely shattered, to a depth of ~5 μm below the surface. Sample was annealed at 800°C before the wear test.

situ-toughened, hot-pressed silicon carbide, ABC-SiC, using 3–72 μm sized diamond abrasives in ambient temperature air, the following conclusions can be made.

(1) Thermal annealing at 1000°–1600°C in argon was found to be effective in enhancing the abrasive wear resistance of ABC-SiC, almost tripling the three-body wear resistance and doubling the two-body resistance, despite the fact that the hardness and (indentation) fracture toughness remained essentially constant. In most annealed conditions, the abrasive wear resistance of ABC-SiC was found to be a factor of two or more than that of commercial SiC (Hexaloy SA, as-received) tested under identical conditions.

(2) Microstructurally, such thermal annealing was found to result in (i) the crystallization of the grain-boundary films above ~1000°C, (ii) the matrix precipitation of aluminum-rich nanoprecipitates (1–5 nm in size) above ~1300°C, and (iii) the accumulation of aluminum in the grain boundaries, with the consequent formation of precipitate-denuded zones with low aluminum concentration adjacent to the grain boundaries, above ~1300°C.

(3) For cases of severe abrasive wear involving the coarse (72 μm) abrasives, the mechanism of wear was associated with near-surface fractures, initiated primarily from grain boundaries, which caused intergranular cracking and grain pullout.

(4) Thermal annealing was found to diminish the incidence of such "coarse abrasive" damage and progressively improve the wear resistance with increased annealing temperature from 1000° to 1600°C. This effect was attributed to the presumed strengthening of the boundaries because of the accumulation of aluminum there. The role of the very fine matrix precipitates was reasoned to be less important because the dimensions of the abrasive particles were far in excess of those of the nanoprecipitates.

(5) For cases of mild abrasive wear involving the fine (3 μm) abrasives, the mechanism of wear was associated primarily with microplowing and mostly transgranular near-surface crack formation (conchoidal cracking damage), with only limited incidence of intergranular cracking and grain pullout.

(6) The effect of thermal annealing was more complex in affecting such mild abrasive wear properties. In general, thermal annealing led to an improvement in the wear resistance of ABC-SiC, an effect likely associated with the local matrix strengthening from the presence of the nanoprecipitates. However, with higher-temperature annealing, the consequent coarsening of these precipitates led to degradation in the wear properties, approaching that of the as-hot-pressed microstructure.

Acknowledgments

Part of this work was made possible through the use of the National Center for Electron Microscopy facility at the Lawrence Berkeley National Laboratory. Thanks are due to Qing Yang for her help in processing the SiC samples.

References

[1]J. J. Cao, W. J. MoberlyChan, L. C. De Jonghe, C. J. Gilbert, and R. O. Ritchie, "*In Situ*-Toughened Silicon Carbide with Al-B-C Additions," *J. Am. Ceram. Soc.*, **79** [2] 461–69 (1996).

[2]C. J. Gilbert, J. J. Cao, L. C. De Jonghe, and R. O. Ritchie, "Crack-Growth Resistance-Curve Behavior in Silicon Carbide: Small versus Long Cracks," *J. Am. Ceram. Soc.*, **80** [9] 2253–61 (1997).

[3]W. J. MoberlyChan, J. J. Cao, C. J. Gilbert, R. O. Ritchie, and L. C. De Jonghe, "The Cubic-to-Hexagonal Transformation to Toughen SiC"; pp. 177–90 in *Ceramic Microstructure: Control at the Atomic Level*. Edited by A. P. Tomsia and A. Glaeser. Plenum Press, New York, 1998.

[4]P. F. Becher, E. Y. Sun, K. P. Plucknett, K. B. Alexander, C. H. Hsueh, H. T. Lin, S. B. Waters, and C. G. Westmoreland, "Microstructural Design of Silicon Nitride with Improved Fracture Toughness: I. Effects of Grain Shape and Size," *J. Am. Ceram. Soc.*, **81** [11] 2821–30 (1998).

[5]H. J. Kleebe, M. K. Cinibulk, R. M. Cannon, and M. Rühle, "Statistical Analysis of the Intergranular Film Thickness in Silicon Nitride Ceramics," *J. Am. Ceram. Soc.*, **76** [8] 1969–77 (1993).

[6]Y. M. Chiang, L. A. Silverman, R. H. French, and R. M. Cannon, "Thin Glass Film between Ultrafine Conductor Particles in Thick-Film Resistors," *J. Am. Ceram. Soc.*, **77** [5] 1143–52 (1994).

[7]Q. Jin, X. G. Ning, D. S. Wilkinson, and G. C. Weatherly, "Redistribution of a Grain-Boundary Glass Phase during Creep of Silicon Nitride Ceramics," *J. Am. Ceram. Soc.*, **80** [3] 685–91 (1997).

[8]Q. Jin, D. S. Wilkinson, and G. C. Weatherly, "High-Resolution Electron Microscopy Investigation of Viscous Flow Creep in a High-Purity Silicon Nitride," *J. Am. Ceram. Soc.*, **82** [6] 1492–96 (1999).

[9]X. F. Zhang, M. E. Sixta, and L. C. De Jonghe, "Grain Boundary Evolution in Hot-Pressed ABC-SiC," *J. Am. Ceram. Soc.*, **83** [11] 2813–20 (2000).

[10]X. F. Zhang, M. E. Sixta, and L. C. De Jonghe, "Diffusion-Controlled Responses to Heat Treatment of Toughened Silicon Carbide," *Defect Diffus. Forum*, **186–187**, 45–60 (2000).

[11]X. F. Zhang, M. E. Sixta, and L. C. De Jonghe, "Nano-Precipitation in Hot-Pressed Silicon Carbide," *J. Mater. Sci.*, **36**, 5447–55 (2001).

[12]T. Senda, E. Yasuda, M. Kaji, and R. C. Bradt, "Effect of Grain Size on the Sliding Wear and Friction of Alumina at Elevated Temperatures," *J. Am. Ceram. Soc.*, **82** [6] 1505–11 (1999).

[13]B. Lawn, N. P. Padture, H. Cai, and F. Guiberteau, "Making Ceramics Ductile," *Science (Washington DC)*, **263** [2] 1114–16 (1994).

[14]X. F. Zhang, M. E. Sixta, and L. C. De Jonghe, "Secondary Phases in Hot-Pressed ABC-Silicon Carbide," *J. Am. Ceram. Soc.*, **84** [4] 813–20 (2001).

[15]P. H. Shipway, "The Role of Test Conditions on the Microabrasive Wear Behaviour of Soda–Lime Glass," *Wear*, **233–235**, 191–99 (1999).

[16]M.-O. Guillou, J. L. Henshall, and R. M. Hooper, "The Measurement of Surface Contact Fatigue and Its Application to Engineering Ceramics," *Mater. Sci. Eng. A.*, **209**, 116–27 (1996).

[17]R. M. L. Foote, Y. W. Mai, and B. Cotterell, "Crack Growth Resistance Curves in Strain-Softening Materials," *J. Mech. Phys. Solids.*, **34** [6] 593–607 (1986).

[18]B. J. Hockey, "Plastic Deformation of Aluminum Oxide by Indentation and Abrasion," *J. Am. Ceram. Soc.*, **54** [5] 223–31 (1971).

[19]J. T. Czernuszka and T. F. Page, "Characterizing the Surface Contact Behavior of Ceramics, Part 2. Chemo-mechanical Effects," *J. Mater. Sci.*, **22**, 3917–23 (1987).

[20]G. S. Painter, P. F. Becher, and E. Y. Sun, "Bond Energetics at Intergranular Interfaces in Alumina-Doped Silicon Nitride," *J. Am. Ceram. Soc.*, **85** [1] 65–67 (2002). □